Simulations of Three-Phase Current Interruptions Through a Black-Box Model of Miniature Circuit Breakers

F. Bizzarri, *Senior Member, IEEE*, L. Ghezzi, M. Maglio, F. Rigamonti and A. Brambilla *Member, IEEE*

***Abstract*—A black-box model for arc based current interruption, originally developed by the same authors for single phase short circuit tests, is here challenged with multipolar circuit breakers in three phase interruptions. Multipolar devices are built by composition of elementary, single pole components. The three phases adopt three replicas of the same single phase model, its parameters having been identified in single pole tests. Splitter-less neutral poles adopt a simplified model, deduced by specialization of the original model after suitably dropping splitter plate features. Various breakers and test cases are considered. Comparisons with experimental results in real short circuit tests show very good agreement, in line with motivating industrial, system-level applications. Indeed, model parameters are obviously single pole design dependent, but they are invariant to different operating conditions and no fine tuning is required to match empirical evidence.**

***Index Terms*—three-phase circuit breaker, miniature circuit breaker, black-box model, circuit breaker simulation.**

I. Introduction

COMPUTATIONALLY light, black-box (BB) circuit breaker models are particularly useful in system-level, low voltage network analyses. Particularly, the transient dynamics of electrical circuits, as soon as an electric fault (typically, a short-circuit) is detected and cleared by a breaker opening maneuver, is of theoretical as well as industrial interest in order to suitably design low voltage systems. The present authors developed in [1] a BB model for single pole circuit breakers, showing good agreement with empirical data and, most of all, invariance of characterizing parameters in other conditions than those used for their identification.

Results were found way superior to those obtained from classical, BB, circuit breaker models, such as, e.g., Mayr [2], Cassie [3], Schwarz [4], Urbanek [5]–[8], or compositions thereof [9], [10]. Particularly, it is empirically found unlikely that classical models adhered with adequate accuracy to different operating conditions, unless refitting their parameters on a case by case basis. This is for example the main drawback of the model proposed in [11], where each pole of the three-phase miniature circuit breaker (MCB) is separately fitted to meet experimental results from a single current interruption. Furthermore, and despite efforts to find local settings to fit individual test curves, agreement with experimental current and voltage time histories is frequently unsatisfactory with said classic models.

The main claim of [1] was the underlying physical basis, although strong simplifications were introduced compared to low level physical adherence of, e.g., magneto-hydro-dynamic (MHD) approaches. The proposed BB model is based onto two pillars, namely air plasma physical behavior in terms of a temperature dependent electrical conductivity law, and a macroscopic description of the arc plasma (inspired by [12]), moving and elongated driven by Lorentz force [13], heated by Ohmic losses and cooled by radiation. The superior behavior of [1] with reference to classical models (the latter originating from high voltage breakers, characterized by remarkably different internal physics) was explained with additional, specific features intentionally introduced to model the physics of low voltage circuit breakers. Precisely, splitter plates introduce surface voltage drops at metal-plasma interfaces, and an outer path circumventing splitters is preferred by the arc until its voltage exceeds that of going through plates [14], [15].

On the other hand, extremely accurate and physically consistent approaches such as MHD resort to very large systems of PDEs (some millions of cells, each cell giving rise to some dozens of equations), supplemented by algebraic closure equations, and thus they are computationally intensive and suffer of very long run time. Thus a single pole complete MHD simulation usually requires hours or days of high performance computing, to be compared with practically real time simulations throughout differential algebraic equation (DAE) based BB models, where around a dozen of equations have to be solved. Despite MHD being practically the only a priori approach when the design of a new circuit breaker pole is concerned, system level studies requiring multipolar devices readily become hardly tractable, or the required effort is disproportionate.

Computational efficiency, along with the beneficial role played by the aforementioned low-voltage breakers characteristic features, motivated the present authors to challenge here the model [1] on multipolar circuit breakers. Each of the three phases inherits a copy of the full model, whose parameters are to be identified in single pole short-circuit tests, once and for all for any single pole type. The neutral conductor, whenever distributed in the electrical system and interrupted in the protective circuit breaker, and when the arc

Federico Bizzarri is with Politecnico di Milano, DEIB, P.zza Leonardo da Vinci, n. 32, I20133 Milano, Italy and also with the Advanced Research Center on Electronic Systems for Information and Communication Technologies E. De Castro (ARCES), University of Bologna, 41026 Bologna, Italy. (e-mail: federico.bizzarri@polimi.it)

Luca Ghezzi, Francesco Rigamonti and Matteo Maglio are with ABB, Viale Dell'Industria 18, I20010 Vittuone, Italy. (e-mail: {luca.ghezzi,francesco.rigamonti,matteo.maglio}@it.abb.com)

Angelo Brambilla is with Politecnico di Milano, DEIB, P.zza Leonardo da Vinci, n. 32, I20133 Milano, Italy. (e-mail: angelo.brambilla@polimi.it)

chamber is not endowed with splitter plates, may be profitably modeled by means of a simplified variant of the original BB element, where a specialization is carried out to remove splitter relevant features from governing equations. (It is understood that three-polar breakers with neutral pole with splitters have to be modeled by means of four copies of the full model.)

In this work, the original model in [1] has also been extended as far as the plasma model is concerned. In particular, the plasma characteristic conductivity law is dynamically computed by resorting also to temperature and pressure dependent electrical conductivity tables, developed at ABB Corporate Research by means of *ab initio* models, describing molecular physics of the gaseous species involved in the air-plasma atmosphere [16], [17]. Said tables are employed at ABB in MHD simulations. As for the application to BB modeling, pressure is arbitrarily fixed and a fitting curve is employed.

In the original version of this BB model [1], the dependence on temperature of the available free charge governing the plasma conductivity was modeled by fitting parameters of $\tanh()$ functions versus generic information available in the literature. The use of this detailed look-up table improves the accuracy of the overall model and mainly the accuracy in modeling the free burning arc of the neutral pole.

The proposed BB model for multipolar circuit breakers is here tested over a variety of test cases deduced from industrial practice. A remarkably good agreement is found with empirical evidence, with current and voltage oscillograms adhering to simulated ones both in terms of time synchronization and amplitudes of electrical quantities.

The outline of this paper is as follows. Section II describes the mathematical model governing phase and neutral poles, while the method for parameter identification is described in Section III. The performance of the model are reported in Section IV, with reference to real three phase short circuit tests and compared with corresponding experimental results. Finally, conclusion are drawn and future research is outlined in Section V.

II. The BLACK-BOX MODEL

The BB model of the arc, which forms in the MCB when the contacts opens, was derived and fully described in [1]. Here we recall the main aspects and cornerstones that allow a straightforward comprehension of how the model works and its usage in the three-phase current interruptions described in Section IV. The reader interested in more details on modeling and simulation of low voltage arcs can refer to [18] and references therein.

The BB model consists of two parts: the plasma model, responsible of the arc dynamics, and the breaker "embedding", i.e., the mechanical, electrical, geometrical parts and material ablation that mutually interact with the plasma and that as a whole drive the arc behaviour in the interruption process. This interaction mainly differentiates an MCB from another.

In developing the air plasma model, we assume that air is composed of the X_2 neutral molecules at T room temperature and pressure, viz. oxygen and nitrogen are viewed as an equivalent molecular diatomic species. The $X_2 \rightarrow X$ dissociation process of such molecules in neutral atoms takes place in the $\mathcal{I}_1 = [T_0, T_1]$ temperature interval. Full dissociation is observed almost at $T = T_1$ and, after increasing temperature above T_1, the first ionization process begins, according to the reaction $\mathrm{X} \rightarrow \mathrm{X}^+ + \mathrm{e}^-$. Assuming that an $(\mathrm{X}^+, \mathrm{e}^-)$ pair is formed from a single X atom, we have $n_{\mathrm{X}^+}(t,T,p) = n_{\mathrm{e}^-}(t,T,p)$, i.e., charge neutrality is always preserved, for any value of temperature and pressure[1]. Thus in the BB model we drop the n_{X^+} species and substitute it with n_{e^-}. The equilibrium values of n_{X} and n_{e^-} at a given T temperature are referred to by using the * notation and are constrained by

$$n^*_{\mathrm{X}}(T) = \Xi\left(1 + \tanh\left(\gamma_{\mathrm{X}}\left(T - \bar{T}_{01}\right)\right)\right) - n^*_{\mathrm{e}^-}(T)\ , \qquad (1)$$

where $\Xi \equiv n^*_{\mathrm{X}_2}(T_0)$, $2\bar{T}_{01} = T_0 + T_1$, and γ_X is a parameter deduced by experimental equilibrium curves. In the model presented in [1], the $n^*_{\mathrm{e}^-}(T)$ function used here, which governs free charge at equilibrium, was implemented according to [19] through a function with a structure similar to (1). In the extended version of the model used to simulate three-phase current interruptions, reported in this paper, it was substituted by a two-dimensional look-up table. Its entries are temperature T and pressure p, its output is the conductance of a normalised volume of plasma.

We decided to use these data to further improve accuracy and mainly to better fit performance of the free burning arc in the neutral pole as better described in the following. Even though the lookup-table is two-dimensional, fixing pressure at a single constant value reveals acceptable. Values from the look-up table are adequately scaled in our implementation.

The BB model is described by the

$$F(v(t), i(t), x(t), P(t), t) = 0,$$

set of DAEs, where $F(v(t), i(t), x(t), P(t), t) =$

$$\begin{cases} \dfrac{dn_{\mathrm{X}}}{dt} - \nu\left(n^*_{\mathrm{X}}(T) - n_{\mathrm{X}}\right) \\ \dfrac{dn_{\mathrm{e}^-}}{dt} - k\left[\dfrac{\left(1 + b(T) n_{\mathrm{e}^-}\right)\left(n^*_{\mathrm{e}^-}(T, p_0)\right)^2 n_{\mathrm{X}}}{\left(1 + b(T) n^*_{\mathrm{e}^-}(T, p_0)\right)\left(\Xi - n^*_{\mathrm{e}^-}(T, p_0)\right)} - n^2_{\mathrm{e}^-}\right] \\ \kappa_1 \dfrac{d^2x}{dt^2} + \kappa_2 \dfrac{dx}{dt} - i^2(t)\chi_{[t_0, +\infty)}(t) \\ i(t) - \dfrac{1/2\left(1 + \tanh(\gamma_s(T - T_1))\right)\sigma n_{\mathrm{e}^-} + g(t)}{x_0 + \min\left(\kappa_3\left(x(t) - x_{\mathrm{sp}}\right)^+, x_{\max}\right)} v(t) \\ g(t) - g_M\left[1 - \dfrac{t - t_0}{\Delta t_s}\chi_{[t_0, t_0 + \Delta t_s]}(t)\right]\chi_{(-\infty, t_0 + \Delta t_s]}(t) \\ \zeta \dfrac{dT}{dt} - \Big[v(t) i(t) - \gamma_r\left(T - T_A\right)^4 - \gamma_c g(t)\left(T - T_A\right) + P(t)\Big]. \end{cases} \qquad (2)$$

The first two expressions of (2) model the dynamic process of dissociation when $T \in \mathcal{I}_1$ and formation of $(\mathrm{X}^+, \mathrm{e}^-)$ pairs when $T > T_1$. To give a simple insight on how free charges form, assume that at $t = t_0$ temperature T steps from $T \ll T_0$ to $T = T^* \gg T_1$. The first expression in Eq. (2) governs the "creation" of $n_X(t)$ dissociated atoms and the second one that of the $n_{\mathrm{e}^-}(t)$ free charges that form the plasma. At equilibrium, say at $t = t^*$, we have $n^*_X(T^*)$ dissociated atoms

[1] Since the model has been developed at fixed pressure, for the sake of simplicity in the following the dependence on p is omitted.

and $2n^*_{\text{e}^-}(T^*)$ free charges in the plasma[2].

The $x(t)$ variable in the third expression in Eq. (2) has a double meaning. Its initial value at the t_0 time instant at which contacts open is $x(t_0) = 0$ and till $x(t) < x_{\text{sp}}$ this variable represents a normalized distance traveled by the arc moving its roots on two almost parallel metal conductors. As soon as $x(t_{\text{sp}}) = x_{\text{sp}}$, it is assumed that the arc touches the splitter plates. For $t > t_{\text{sp}}$, the $x(t)$ variable represents the normalized length of the plasma meanders around splitter plates. In both cases the dynamic evolution of $x(t)$ is forced by the $i^2(t)$ term standing for (normalized) Lorentz force[3]. The fitting parameters κ_1 and κ_2 are breaker dependent. As a consequence, the denominator of the first algebraic equation in Eq. (2) can be interpreted as follows[4]. For $t < t_{\text{sp}}$ the arc travels towards the splitter plate but its length is fixed to x_0. When the splitter plates are reached the length of the arc becomes $x_0 + \kappa_3(x(t) - x_{\text{sp}})$ till a maximum (fitting) value $x_{\max}$ is reached (κ_3 is a proper scaling factor).

The fourth expression in Eq. (2) models the $i(t)$ arc current as function of the $v(t)$ arc voltage, which are linked by a variable conductance, and mainly the $n_{\text{e}^-}(t)$ (normalized) free charges. The σ parameter governs arc conductance. The term $1/2\,(1 + \tanh(\gamma_s(T - T_1)))$ is a numerical expedient to wipe out free charges when the arc quenches (only dissociated atoms exist). The $g(t)$ contribution to conductance evolves according to the fifth expression in Eq. (2), where g_M is the value when the contacts are closed and models an ideal opening of the metallic contacts that does not involve arcing. When the metallic contacts of the breaker are closed, the $g(t) = g_M$ function dominates $\sigma n_{\text{e}^-}(t)$ and gives the main contribution to the conductance of the breaker. During contact separation, which is assumed to have constant speed, the conductance of the metal contacts drops, with $g(t)$ decreasing from g_M to 0 along the Δt_s separation time interval. As evident from summing the two contributions to conductance, two resistors are assumed to coexist in parallel connection, they always remain active in the model, and their actual value determines which one practically describes the conductance of the MCB, the other taking negligible values.

The sixth expression of Eq. (2) is an energy balance governing the T plasma temperature. The $v(t)i(t)$ term accounts for Joule heating. The $\gamma_r\,(T - T_A)^4$ term models dissipation by radiation, γ_r is a fitting parameter and T_A is the "reference" temperature (not necessarily the room temperature). The $\gamma_c g(t)\,(T - T_A)$ term is an expedient with no direct physical meaning used to control the arc ignition phase by fictitiously lowering the arc temperature just after arc ignition. The $P(t)$ term is introduced since the plasma can be split into several sections and power may flow from one section to another. The $P(t)$ function is tailored in each case and accounts for this power exchange as exemplified in Sec. II-A for the considered case study.

[2]It is worth noticing that actually the equilibrium is asymptotically reached as far as $t \to \infty$ but from the practical view point it is reasonable to identify a time instant $t = t^*$.

[3]The $\chi_{\mathcal{I}}(x)$ indicator or characteristic function of the generic $\mathcal{I}$ interval is such that $\chi_{\mathcal{I}}(x) = 1$ if $x \in \mathcal{I}$ and $\chi_{\mathcal{I}}(x) = 0$ if $x \notin \mathcal{I}$.

[4]The $^+$ symbol stands for the positive part of a real.

A. Phase pole model

We consider a pole of a three-phase breaker. During current interruption, as soon as contacts open, arcs immediately form between them. The breaker design is such that the arc is pushed towards splitter plates as fast as possible by Lorentz forces due to the increasing short-circuit current and by internal pressure. When the arc touches the splitter plates it starts splitting into two parts, one forming meanders around the splitters and the other flowing through them. In a well designed breaker, the plasma outside the splitter plates is unstable and quickly quenches while that inside the splitter plates fully carries the short-circuit current. Surface resistance at plasma-metal interfaces increases arc impedance, thus increasing arc voltage drop, limiting current and anticipating the current zero. In a successful interruption, arc temperature after current zero is not enough to sustain a new restrike.

This dynamical splitting effect is modeled by using two plasma sections[5], each described by Eq. (2), that exchange the $P(t)$ power and an additional equivalent circuit that models the arc roots that form on splitter plates. Once more, a detailed description is found in [1].

B. Neutral pole model

The design of the neutral pole is simpler and less critical than that of the three-phase pole. It does not have the splitter plates and thus the possible arc forming after the contact opening remains and burns between the separating contacts until it quenches. In this case we use only one instance of the model described by Eq. (2) and the dynamical evolution of $x(t)$ is revised since the neutral pole does not have arc runners and Lorentz force driven arc elongation is neglected thus $x(t)$ is the distance between contacts (i.e., the arc length). The latter are assumed to separate at constant speed during a fixed time interval Δt_c and reach a geometry dependent maximum value $x_{\max}$. In this case, x_0 is chosen to be very small, and

$$x(t) = \min\left(x_0 + \frac{(t - t_0)x_{\max}}{\Delta t_c}, x_{\max}\right), \qquad (3)$$

thus (i) dropping the third expression in (2) and (ii) replacing the denominator of the fourth expression in (2) with (3). Also in this case, to have an adequately accurate modeling of the voltage that develops across this arc, the model previously presented in [1] was enhanced by substituting the $n^*_{\text{e}^-}(T)$ fitting function with the $n^*_{\text{e}^-}(T, p)$ look-up table mentioned in Sec. II.

III. Model fitting

Since we assume three-phase breakers are obtained by mechanically coupling three identical single phase poles, fitting is done by considering only one pole and it is thus performed by exploiting experimental results from single-phase current interruptions. The same fitted model is used in the three-phase version of the breaker. We performed fitting by using experimental data, which is obviously the best situation. However, fitting can be in principle performed also versus a set of numerical results by MHD simulations used, for instance, to develop the MCB.

[5]As far as the section non entering the splitter plate is concerned, $x_{\text{sp}} = 0$.

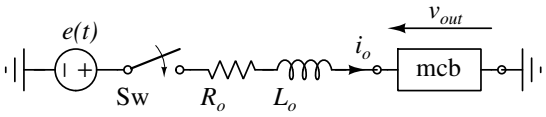


Figure 1. Schematic of the circuit used to fit the parameters of the phase pole of the breaker.

A. The fitting of the phase pole

The schematic of the circuit used in the single-phase current interruption is shown in Fig. 1. The $e(t) = E_o \sin(2\pi\, 50t)$ independent voltage source, the R_o resistance and L_o inductance model the lab circuit used for short-circuit testing. Given the E_o value (almost always $230\sqrt{2}$), the values of R_o and L_o determine the prospective current and the $\cos(\phi)$ of the circuit. Short-circuit is applied by closing the Sw auxiliary switch, the MCB pole already being closed.

To fit the model parameters we used a version of the derivative-free "simplex" optimization method, originally described in [20]. Since during current interruptions the shape of current is largely influenced by the shape of the voltage waveform, we chose to minimize the model-experiment discrepancy on the $v_{out}(t_k)$ voltage shown in Fig. 1, sampled on an even grid $\mathcal{K}$ of time samples that span the interval of the experimental current interruption. The nonlinear cost function is defined as

$$c(p) = \sum_{t_k \in \mathcal{K}} \left(v_{out}(t_k, \beta) - v_{\exp}(t_k, \beta)\right)^2 , \qquad (4)$$

where β is the parameter vector and the $v_{\exp}(t_k, beta)$ is derived from experimental voltages. Several experimental current interruptions with the same prospective current were considered, the sampled voltage across the MCB was recorded and filtered by the Savitsky-Golay method to remove voltage spikes and noise. The $v_{\exp}(t_k, \beta)$ function is the local average voltage waveform over a small neighborhood of t_k, as output by the filter.

We initially performed some parameter tentative fitting by hand. After an adequate initial guess tentative is found, we run the simplex optimization method. The parameter vector is $\beta = [\kappa_1, \kappa_2, \sigma_o, \sigma_s, v_d, \zeta, \gamma_r]$. By referring to Eq. (2), the κ_1 and κ_2 parameters govern the arc length and its inception into splitter plates, $\sigma_{o,s}$ scales the conductances of the two sections of the plasma, v_d is the total voltage drop due to arc roots on splitter plates, ζ governs the dynamic behavior of the plasma equivalent temperature and finally γ_r governs power radiated by the arc. See Table I in [1] for a detailed explanation of the meaning and effects of the parameter vector entries.

In this paper, we consider two different types of three-phase MCBs, that we refer to as TY1 and TY2. Their main characteristics are $V_n = 400\,\mathrm{V}$ (nominal voltage) and $I_n = 32\,\mathrm{A}$ (nominal current) for both, $I_{cn} = 10\,\mathrm{kA}$ (rated short circuit capacity) for TY1 and $I_{cn} = 6\,\mathrm{kA}$ for TY2.

For both types, optimizations were performed on sets of experimental results at $6\,\mathrm{kA}$ prospective current. Simplex optimization converges to a local minimum in about 20 iterations and requires a slightly higher number of evaluations of the $c(\beta)$ cost function. The complete optimization flow runs in about $3\,\mathrm{s}$. All simulations carried out in this work were performed on a LINUX-INTEL-I7 $3.2\,\mathrm{GHz}$ computer.

B. The fitting of the neutral pole

The neutral pole is separately fitted since, as said, its design differs from that of the phase pole. The neutral pole is fitted by using the simulation circuit shown in Fig. 2. The $A_o(t)$ independent current source drives the P_N neutral pole by replicating the current recorded from experiments. Experimental currents were recorded during single-phase interruption where the neutral pole is connected in series to the phase pole.

The parameters of the neutral pole model are fitted in order to minimize the discrepancy error between the $v_N(t)$ experimental and the simulated voltages across the pole. We used the same Eq. (4) cost function; the parameter vector is $\beta = [\sigma, \zeta, \gamma_r, \Delta t_c]$, where σ scales the plasma conductance[6] and Δt_c is the time interval for the contacts separation at constant speed. In Fig. 3 we show the resulting $v_N(t)$ simulated voltage after fitting and the corresponding experimental voltage of the TY1 breaker type. It is worth noticing that we modeled the neutral poles of the TY1 and TY2 MCBs as identical, since in the considered short circuit range, according to experimental measurements, the neutral behavior is equivalent.

IV. Numerical vs experimental results

The breaker's mechanical design includes actuators kinematic chains and a transmission shaft that moves the contacts of the three phases and the neutral. Any of the three phases may trigger the others and the neutral, as soon as the corresponding phase current exceeds a threshold $i_{\max}$ at time t_{tr}. After a mechanical delay Δt_d, arcing begins at $t_0 = t_{\mathrm{tr}} + \Delta t_d$ on the three phases. The neutral pole is further delayed by an intentional Δt_n.

The schematic of the equivalent experimental circuit used to simulate the reported three-phase current interruptions is shown in Fig. 4. At the t_s time instant the $S_{a,b,c}$ auxiliary switches are simultaneously closed and short-circuit begins. The t_s time instant is chosen according to standard prescribed insertion angles. The short-circuit is cleared by the opening of the three-phase MCB under test, labeled as "3P+N mcb" in Fig. 4. The $R_{a,b,c}$ resistances and $L_{a,b,c}$ inductances set the peak value of the prospective current and the desired $\cos(\phi)$ of the circuit. The prospective current, the insertion angle and

[6] As stated in Section II, the $n^*_{\mathrm{e}^-}(T, p)$ function used to govern free charge at equilibrium (see (1)), was implemented by a two-dimensional look-up table whose output is the conductance of a *normalised volume* of plasma. The constant σ is thus used since the arc actually occupies a given volume whose cross-section neither belongs to the model parameters nor appears in (2).

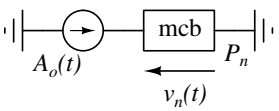


Figure 2. Schematic of the circuit used to fit the parameters of the neutral pole breaker.

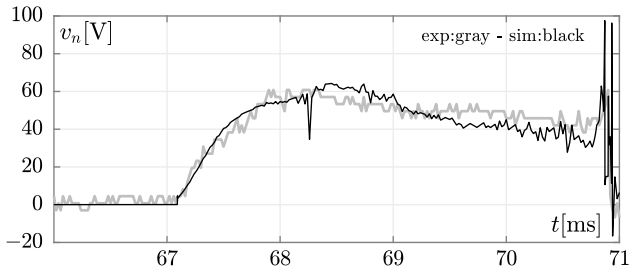


Figure 3. The arc voltage of the neutral pole of the TY1 breaker. The gray trace is the experimental one, the black trace is the simulated one.

the $\cos(\phi)$ of each experiment are reported in corresponding figure captions.

We first describe the results obtained by using the TY1 breaker model. In Fig. 5 we report the experimental and simulation results of a $4.5\,\mathrm{kA}$ prospective current interruption. The auxiliary switches are closed at $t_s = 98.5\,\mathrm{ms}$ and phase c current (panel (c)) is the first to cross the $i_{\max} = 200\,\mathrm{A}$ threshold at $t_{\mathrm{tr}} = 98.575\,\mathrm{ms}$. In this breaker, we have $\Delta t_d = 1\,\mathrm{ms}$ and $\Delta t_n = 0$ and thus contacts in all poles start separating at $t_{\mathrm{tr}} + \Delta t_d = 99.575\,\mathrm{ms}$. By observing the voltage waveforms shown in Fig. 5(e)–(g)[7], we see that arc voltage increases due to arc length increase and arc motion towards splitter plates. The first arc to enter splitter plates is that of phase c. This is visible since arc voltage quickly jumps at about $400\,\mathrm{V}$ (absolute value). Current limitation takes place thereafter. Note that during the time interval from contact opening to phase c arc entering splitter plates, there is a relatively small current flow through the neutral pole. This current falls to 0 and the neutral arc quenches when phase b arc enters the splitter plates. After a short time interval also the phase a arc enters the splitter plates and then that of phase b. The arc of phase a is the first to quench. The MCB enters a bi-phase conduction mode and finally at $105\,\mathrm{ms}$ the remaining two arcs quench and the current interruption process successfully ends. It is worth noticing that simulation results agree very well with the experimental ones for all current and voltage waveforms.

[7]In all the following figures, the i_n current will be displayed only as a result of numerical simulations. This is due to the fact that a current sensor was not used to experimentally measure the i_n current. Furthermore, obtaining it as the sum of the phase currents yields a vary noise oscillogram, also having in mind that i_n is typically lower than the phase currents.

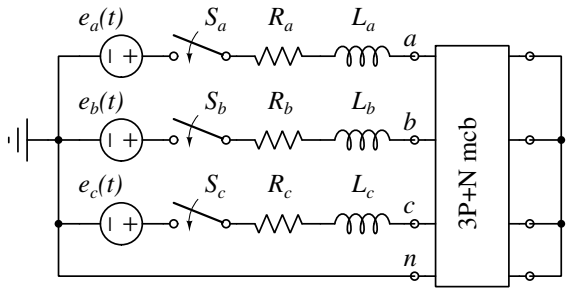


Figure 4. The schematic of the three-phase plus neutral test circuit.

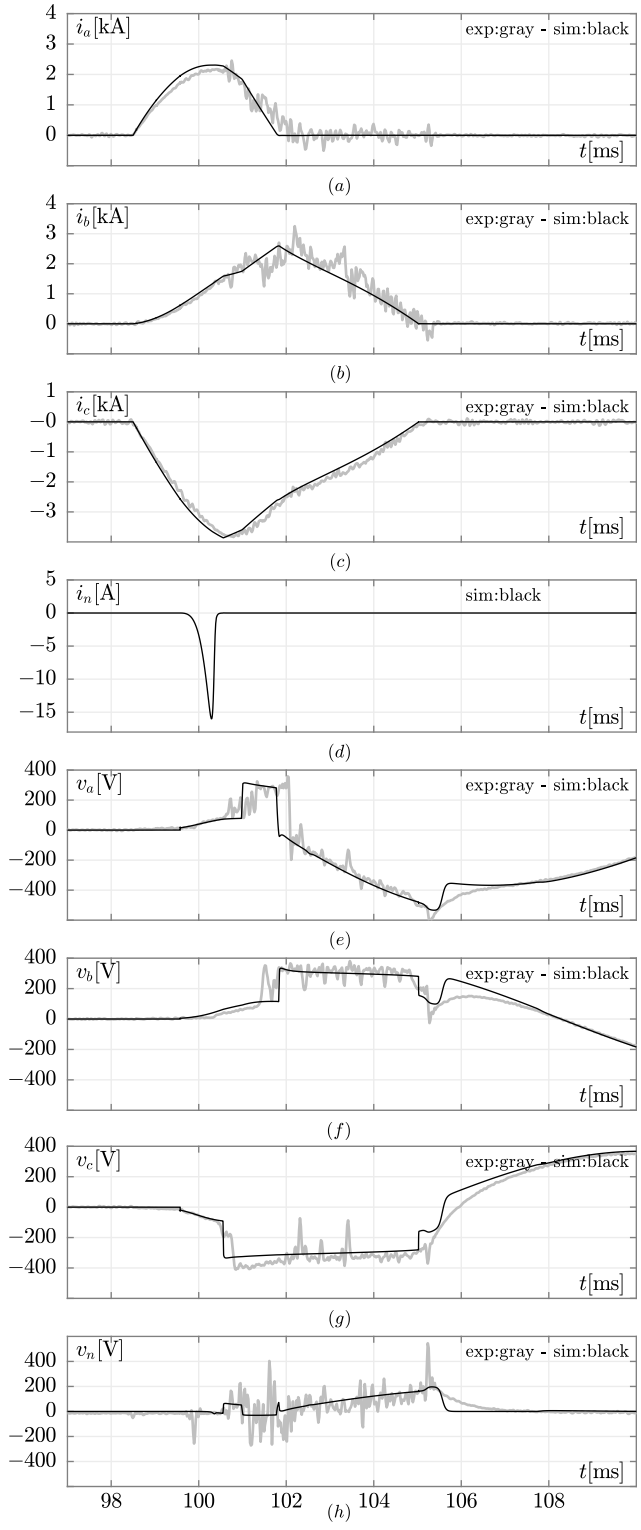


Figure 5. TY1 breaker. Prospecting current $4.5\,\mathrm{kA}$, insertion angle $120°$, $\cos(\phi) = 0.75$.

We used the same breaker model, i.e., with exactly the same parameter values, to simulate two different current interruptions with increasing prospective current values. In Fig. 6, we show the results with a prospective current of $6\,\mathrm{kA}$. It is immediate to appreciate once more the very good agreement

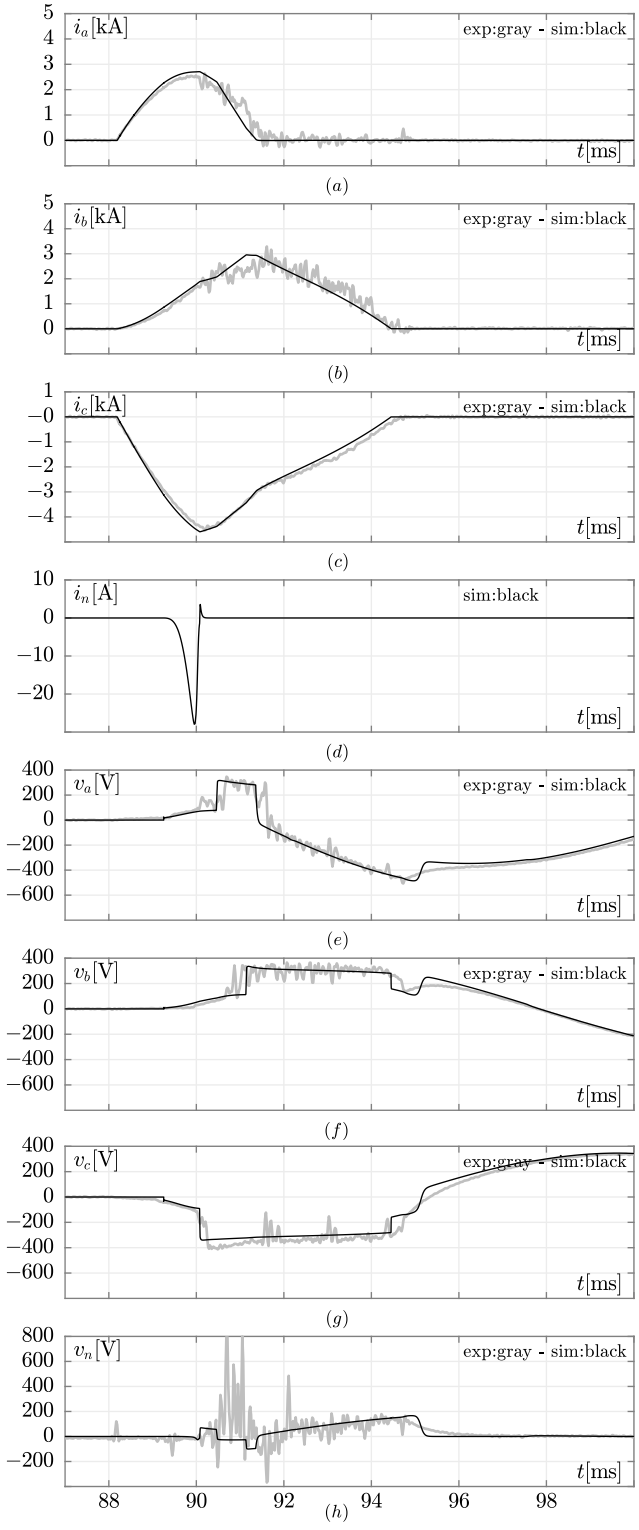


Figure 6. TY1 breaker. Prospective current 6 kA, insertion angle 120°, $\cos(\phi) = 0.65$.

between the set of simulated waveforms and the experimental ones. Since the insertion angle is the same as the previous current interruption, the timing sequence of the various events remains the same. What changes are the peak values of phase currents and the arc current of the neutral pole. Its current

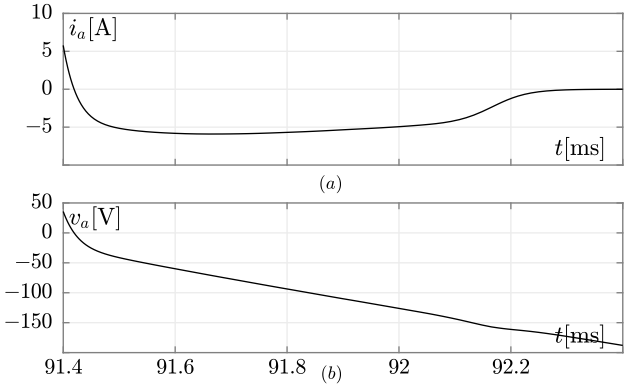


Figure 7. Zero crossing of the current in the a phase of the TY1 breaker. The waveforms shown in this figure are an enlargement of the corresponding ones shown in Fig. 6(a) and (e). (a): arc current [A]. (b): arc voltage [V].

zero crossing without arc quenching is clearly visible; during current zero crossing the arc dynamics is mainly governed by the first two equations of (2). (the prey-predator model described in [1] and inspired by [12]). This aspect of the model is better evidenced in Fig. 7, which is an enlargement of the current (panel (a)) and voltage (panel (b)) waveforms of phase a shown in Fig. 6(a) and (e), when they cross zero. The arc current crosses zero and the arc voltage reverses; it thus makes a dip and then goes back toward zero. This happens in about 150 µs. Arc temperature quickly drops and so do free-charges and the residual current. Current drops to less than 10 mA after 1 ms from zero crossing.

The waveforms of the last current interruption test that we report on the TY1 breaker model are shown in Fig. 8. In this case the prospective current is 10 kA. The insertion angle is 45° and thus the timing of the opening differs from that of the previous two cases. Once more we can appreciate that simulation and experimental results agree very well.

The results reported in Fig. 5, Fig. 6 and Fig. 8 clearly show that the proposed model well covers different working conditions, that is, it covers the entire range of prospective currents in short-circuit tests with a case-invariant (albeit breaker-dependent) set of model parameters. We recall that all simulations employ the same set of parameters, identified once and for all in a single phase training test case.

The other mandatory request for a good and reliable use of a BB model is that it adapts to different types of breaker design. As anticipated, we considered a different model of MCB. The TY2 MCB is designed so that the arc travels toward the splitters faster than in the TY1 model; a larger number of plates forces a higher voltage across the pole, improving current limitation.

The simulation results of the TY2 breaker are shown in Fig. 9. As for TY1 MCB, the parameters of the phase pole model were fitted on a set of single phase experimental current interruptions. The current interruption in Fig. 9 refers to the 6 kA prospective current, since this is the TY2 rated short-circuit capacity. Results are reported differently than in previous figures. Each of the latter refers to a single current interruption, while in Fig. 9 we report several experimental interruptions at the same prospective current.

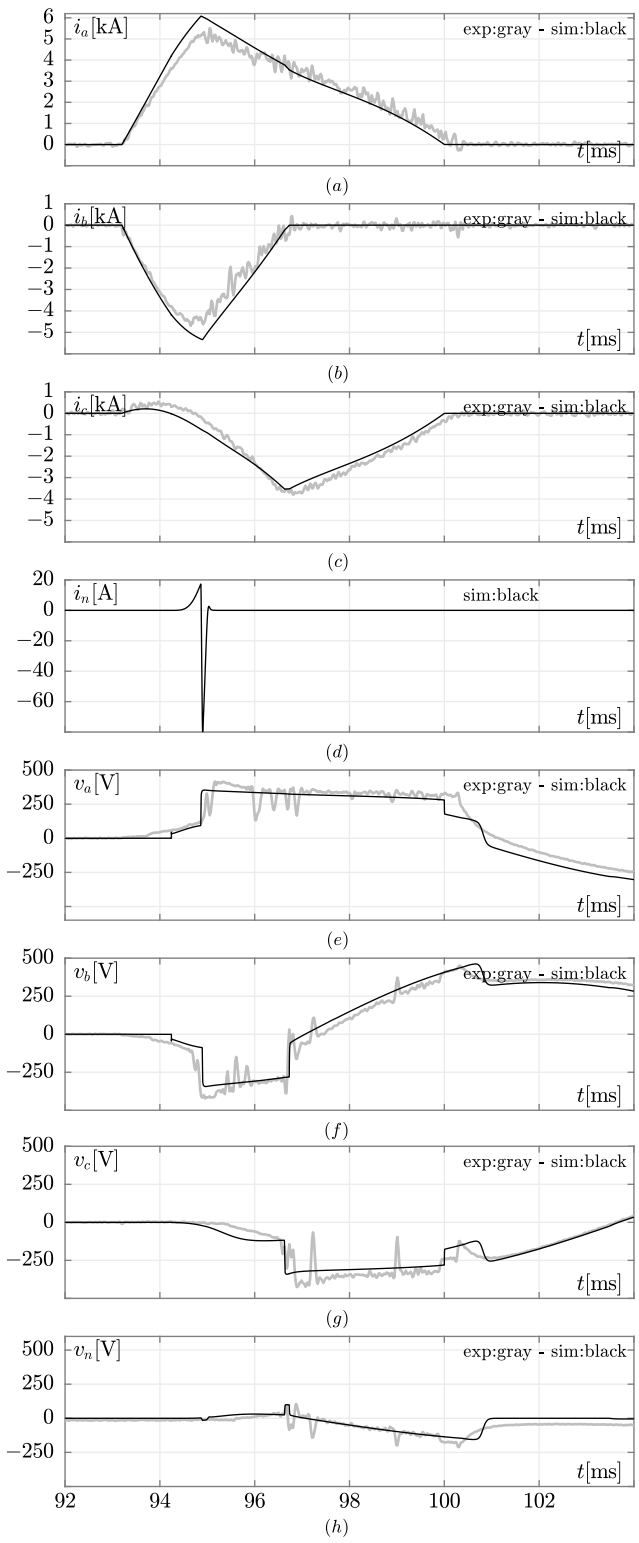


Figure 8. TY1 breaker. Prospective current 10 kA, insertion angle 45°, $\cos(\phi) = 0.5$.

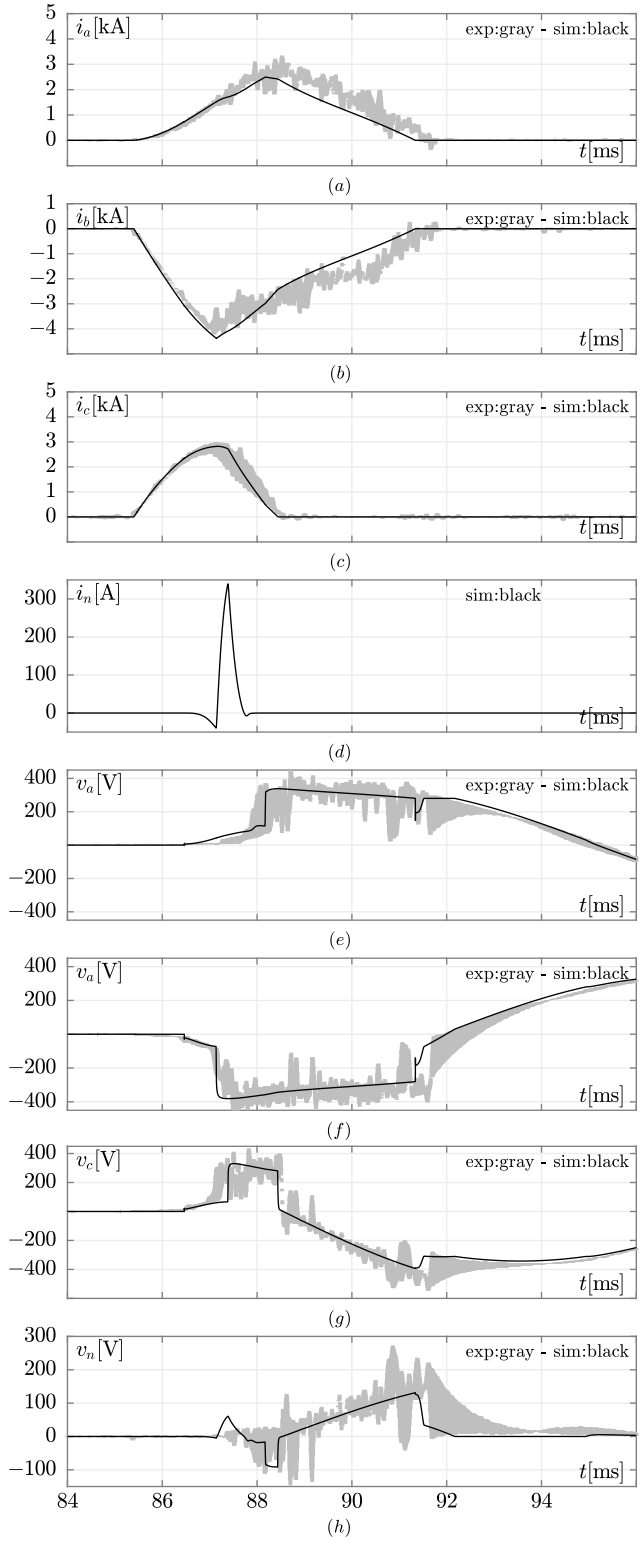


Figure 9. TY2 breaker. Prospective current 6 kA, insertion angle 0°, $\cos(\phi) = 0.65$. Gray areas are the regions enclosed by the upper and lower enveloping waveforms obtained from experimental currents/voltages recorded on a set of identical MCBs interrupting the same 6 kA prospective current in the same experimental setup. Variability of the arc behaviour leads to these different current/voltage experimental waveforms. In the best situation, the simulated waveforms should fall inside the gray areas.

The well-known experimental dispersion is marked by tracing an upper and a lower envelope, formally defined $\forall t \in \Delta\mathcal{T}$ as $i^{\mathrm{u}} := \max_{j\in\mathcal{S}}\{i_j(t)\}$ and $i^{\mathrm{l}} := \min_{j\in\mathcal{S}}\{i_j(t)\}$ respectively, where $\mathcal{S}$ is the (finite) set of experimental currents sampled at the t time instants collected in the set $\mathcal{T}$. By construction, all experimental curves fall in the bands therein. Simulated arc current and voltage waveforms are expected to lay in these

bands too. By considering Fig. 9 and for example the arc current of the a phase we see the upper and lower bands extracted from the set of experimental waveforms and that the simulated current is practically inside this band. Arc voltages behave analogously. It is also evident that the voltage steps when the arcs enter splitter plates fall almost perfectly in the voltage bands.

To show in a synthetic way the different behavior of the two types of MCBs, we compute the $\mathrm{I}^2\mathrm{t}_k = \int_{\Delta T} i_k^2(\tau)d\tau$ value (for $k \in \{a, b, c\}$) for both breakers interrupting the same $6\,\mathrm{kA}$ prospective current, with the same insertion angle. Results are reported in Table I (corresponding phases are suitably grouped for the two interruptions); since TY2 MCB is "faster" than TY1 it has higher limiting characteristics and this leads to a lower $\mathrm{I}^2\mathrm{t}_k$ (for $k \in \{a, b, c\}$). This result shows that the proposed model well adapts to fit different MCBs.

CPU times never exceeded $2\,\mathrm{s}$ and thus we underline the high numerical efficiency of the model.

V. Conclusions

The circuit breaker model with arc based interruption originally developed in [1] for unipolar devices has been successfully challenged on three phase short-circuit tests. Agreement with experimental current and voltage waveforms perfectly meets the needs of industrial practice in circuit breaker engineering. This result is deemed excellent by ABB, the industrial partner participating to this research, because the same settings as used for single pole interruptions have been ported, unaltered, to multipolar tests. Additionally, a simplified, splitter-less model for neutral poles has been deduced easily from the more general, original model. Also in this case, results are more than satisfactory.

Since the proposed model is BB, it is inherently a posteriori to the development of the individual circuit breaker being tested, meaning that different poles must be fitted individually. Nonetheless, the present paper brings evidence that the behavior of a complex breaker may be deduced by BB models of its poles, and that model settings are invariant to changes in operating conditions, within an industrially acceptable accuracy.

Boosted by the positive results here collected, the authors plan to use the model to study the behavior of two circuit breakers in coordination tests. Particularly, a first envisaged system-level application are selectivity tests, where a first, downstream circuit breaker must clear a fault while a second, upstream circuit breaker must remain closed. As a second coordination application, back-up tests will be analyzed, where the interruption capability of a first, downstream circuit breaker is enhanced owing to the cooperation of a second, upstream circuit breaker that is designed to open together with the former. Our goal is to synthetically test as many coordination cases as possible, i.e., as long as simulations yield unequivocal conclusions, in order to help fill selectivity and back-up tables in. This interest is motivated by the potentially consistent savings that circuit breaker industry may achieve reducing the number of extremely time consuming lab tests.

The industrial circuit breakers motivating this study are known to be virtually unaffected by arc re-strikes, after the current zero has been reached. Future research could aim at generalizing the black-box model so to include a thermo-electric dielectric break-down criterion. The task is complicated by local effects, such as geometrical singularities inducing electric field peaks, in addition to the thermal dynamics of the conductive channel.

Table I
$\mathrm{I}^2\mathrm{t}_k$ (FOR $k \in \{a, b, c\}$) OF MCBS INTERRUPTING $6\,\mathrm{kA}$.

	TY1		TY2	
phase	**Sim**	**Exp**	**Sim**	**Exp**
a	11599	10830	12020	17553
b	19229	19114	35048	35476
c	46747	46402	11188	10692

References

[1] F. Bizzarri, A. M. Brambilla, L. Ghezzi, and F. Rigamonti, "Circuit level model of miniature circuit breakers," *IEEE Transactions on Power Delivery*, vol. 33, no. 6, pp. 2700–2709, Dec 2018.

[2] O. Mayr, "Beiträge zur theorie des statischen und des dynamischen lichtbogens," *Archiv für Elektrotechnik*, vol. 37, no. 12, pp. 588–608, 1943.

[3] A. Cassie, "Arc rupture and circuit severity theorie nouvelle des arcs de rupture et de la rigidite des circuits," *CIGRE Report, Paris*, no. 102, 1939.

[4] J. Schwarz, "Dynamisches verhalten eines gasbeblasenen, turbulenzbestimmten schaltlichtbogens," *ETZ-A*, vol. Bd. 92, pp. 389–391, 1971.

[5] W. Rieder and J. Urbanek, "New aspects of current zero research on circuit breaker reignition. A theory of thermal non-equilibrium arc conditions," *CIGRE Report, Paris*, no. 107, 1966.

[6] J. Urbanek, "The time constant of high voltage circuit breaker arcs before current zero," *Proceedings of the IEEE*, vol. 59, no. 4, pp. 502–508, 1971.

[7] F. Bizzarri and A. Brambilla, "Brushing up on the Urbanek black box arc model," *IEEE Transactions on Circuits and Systems I: Regular Papers*, vol. 65, no. 5, pp. 1675–1683, May 2018.

[8] F. Bizzarri, A. Brambilla, L. Ghezzi, and F. Rigamonti, "The Urbanek black box arc model in passive resonance circuit breakers for HVDC applications," in *2018 IEEE International Symposium on Circuits and Systems (ISCAS)*, May 2018, pp. 1–5.

[9] V. Rashtchi, A. Lotfi, and A. Mousavi, "Identification of KEMA arc model parameters in high voltage circuit breaker by using of genetic algorithm," in *Power and Energy Conference, 2008. PECon 2008. IEEE 2nd International*, Dec 2008, pp. 1515–1517.

[10] CIGRE Working Group 13.01, "Applications of black box modelling to circuit breakers," *Electra*, no. 149, pp. 40–71, 1993.

[11] H. Wu, L. Yuan, L. Sun, and X. Li, "Modeling of current-limiting circuit breakers for the calculation of short-circuit current," *IEEE Transactions on Power Delivery*, vol. 30, no. 2, pp. 652–656, April 2015.

[12] D. McKenzie and A. Ross, "Predator-prey dynamics stabilised by non-linearity explain oscillations in dust-forming plasmas," *Nature/Scientific Reports*, vol. 6, no. 24040, April 2016.

[13] V. Terzija, G. Preston, M. Popov, and N. Terzija, "New static "airarc" emtp model of long arc in free air," *IEEE Transactions on Power Delivery*, vol. 26, no. 3, pp. 1344–1353, July 2011.

[14] M. Lindmayer, E. Marzahn, A. Mutzke, T. Ruther, and M. Springstubbe, "The process of arc splitting between metal plates in low voltage arc chutes," *IEEE Transactions on Components and Packaging Technologies*, vol. 29, no. 2, pp. 310–317, June 2006.

[15] J. W. McBride and P. M. Weaver, "Review of arcing phenomena in low voltage current limiting circuit breakers," *IEE Proceedings - Science, Measurement and Technology*, vol. 148, no. 1, pp. 1–7, Jan 2001.

[16] W. Smith and R. Missen, *Chemical reaction equilibrium analysis: theory and algorithms*, ser. Wiley series in chemical engineering. Wiley, 1982.

[17] M. Capitelli, G. Colonna, and A. D'Angola, *Fundamental aspects of plasma chemical physics - thermodynamics*, ser. Springer Series on Atomic, Optical, and Plasma Physics. New York: Springer-Verlag, 2012.

[18] A. Balestrero and L. Ghezzi, "Modeling and simulation of low voltage arcs," Ph.D. dissertation, TU Delft, 2010, adv. Prof. L. van der Sluis.

[19] W. Rieder, *Plasma und Lichtbogen*, ser. Hochschul-Lehrbuch. Vieweg, 1967.
[20] J. A. Nelder and R. Mead, "A simplex method for function minimization," *Computer Journal*, vol. 7, pp. 308–315, 1965.



Federico Bizzarri (M'12–SM'14) was born in Genoa, Italy, in 1974. He received the Laurea (M.Sc.) five-year degree (*summa cum laude*) in electronic engineering and the Ph.D. degree in electrical engineering from the University of Genoa, Genoa, Italy, in 1998 and 2001, respectively. Since October 2018 he has been an associate professor at the Electronic and Information Department of the Politecnico di Milano, Milan, Italy. He is a research fellow of the Advanced Research Center on Electronic Systems for Information and Communication Technologies "E. De Castro" (ARCES), University of Bologna, Italy. He served as an Associate Editor of the IEEE Transactions on Circuits and Systems — Part I from 2012 to 2015 and he was awarded as one of the 2012-2013 Best Associate Editors of this journal.



Luca Ghezzi received a M.Sc. in civil engineering from the Technical University (Politecnico) of Milano, Italy (1998), a M.Sc. in mathematics from the University of Milano, Italy (2007), and a Ph.D. in electrotechnology from the Technical University of Delft, the Netherlands (2010). He works for ABB, involved in modeling and simulation of, a.o., electric arcs, approached both with multiphysics and at circuit level.



Matteo Maglio received the M.Sc. degree in electrical engineering from Politecnico di Milano (Milano, Italy) in 2009, and the Ph.D. degree in electrical engineering from Politecnico di Milano (Milano, Italy) in 2013 working on electrical machines and railway system diagnostic tools. He joined ABB in 2013 and his activities are related to electrical system simulation and low voltage circuit breakers design.



Francesco Rigamonti received the M.Sc. degree in nuclear physics from Universitá degli studi di Pavia (Pavia, Italy), working on nuclear photoreactions on polarized targets. In 2011 he joined ABB and, in parallel, in 2017 he received his executive Ph.D. in electrical engineering at Politecnico di Milano (Milan, Italy), focused on magnetic inverse problem applied to low voltage breakers. His work mainly regards physical modelling and computational aspects of low voltage electric arc.



Angelo Brambilla (M'16) received the Dr. Ing. degree in electronics engineering from the University of Pavia, Pavia, Italy, in 1986. He is full professor at the Dipartimento di Elettronica, Informazione e Bioingegnaria, Politecnico di Milano, Milano, Italy, where he has been working in the areas of circuit analysis, simulation and modeling.